# Linearized Tensor Renormalization Group Algorithm for the Calculation of Thermodynamic Properties of Quantum Lattice Models

Wei Li,[1] Shi-Ju Ran,[1] Shou-Shu Gong,[1] Yang Zhao,[1] Bin Xi,[1] Fei Ye,[2] and Gang Su[1,*]

[1]College of Physical Sciences, Graduate University of Chinese Academy of Sciences, P. O. Box 4588, Beijing 100049, China
[2]College of Materials Science and Opto-Electronic Technology, Graduate University of Chinese Academy of Sciences, P.O. Box 4588, Beijing 100049, China

(Received 21 November 2010; revised manuscript received 21 February 2011; published 22 March 2011)

A linearized tensor renormalization group algorithm is developed to calculate the thermodynamic properties of low-dimensional quantum lattice models. This new approach employs the infinite time-evolving block decimation technique, and allows for treating directly the transfer-matrix tensor network that makes it more scalable. To illustrate the performance, the thermodynamic quantities of the quantum $XY$ spin chain as well as the Heisenberg antiferromagnet on a honeycomb lattice are calculated by the linearized tensor renormalization group method, showing the pronounced precision and high efficiency.

DOI: 10.1103/PhysRevLett.106.127202 PACS numbers: 75.10.Jm, 02.70.−c, 05.30.−d, 75.40.Mg

Since the appearance of White's density-matrix renormalization group (DMRG) theory [1], the numerical renormalization group (RG) approaches have achieved great success in studying low-dimensional strongly correlated lattice models [2]. In the past few years, a number of RG-based methods, e.g., the coarse-graining tensor renormalization group (TRG) [3–5], projected entangled pair states [6], entanglement renormalization [7], the infinite time-evolving block decimation (iTEBD) [8], finite-temperature DMRG [9,10], etc., have been proposed. In spite of the great success in one- and two-dimensional (1D and 2D) lattice models, it is still quite necessary to develop new algorithms to improve the accuracy and efficiency of numerical calculations for strongly correlated systems.

In this Letter, we propose a new algorithm to simulate the thermodynamics of low-dimensional quantum lattice models. Our strategy is first to transform the $D$-dimensional quantum lattice model to a $(D+1)$-dimensional classical tensor network by means of the Trotter-Suzuki decomposition [11], and then to decimate linearly the tensors following the lines developed in the iTEBD scheme to obtain the thermodynamics of the original quantum many-body system. This algorithm is so dubbed as the linearized TRG (LTRG). As is known, the previous real space TRG approach deals with the 2D tensor network with exponential decimation in the coarse-graining procedure, which was shown effective for both 2D classical and quantum lattice models [4,5,12–15]. For the best illustration of the algorithm and performance of the LTRG approach, we take the exactly solvable 1D quantum $XY$ spin chain as a prototype. The results show that the precision of the LTRG method is comparable with that of the transfer-matrix renormalization group (TMRG) [16], the method that is quite powerful for simulating the 1D quantum lattice models at finite temperatures (e.g., Refs. [17,18]). To demonstrate its scalability, a LTRG result with remarkable precision for a 2D spin-1/2 Heisenberg antiferromagnet on a honeycomb lattice is also included.

Let us start with the Hamiltonian of a 1D quantum many-body model given by

$$H=\sum_{i=1}^{N}h_{i,i+1}=H_1+H_2,\qquad H_1=\sum_{i=1}^{N/2}h_{2i-1,2i},\qquad H_2=\sum_{i=1}^{N/2}h_{2i,2i+1},\tag{1}$$

where $N$ (even) is the number of sites. By inserting $2K$ (large $K$) complete sets of states $\{|\sigma_i^j\rangle\}(\sigma_i^j=1,\cdots,D)$ with $i$ the site index and $j$ the Trotter index, the partition function of this model can be represented as

$$\begin{aligned}Z_N&\simeq \mathrm{Tr}[e^{-\beta H_1/K}e^{-\beta H_2/K}]^K\\&=\sum_{\{\sigma_i^j\}}\prod_{j=1}^{K}\langle\sigma_1^{2j-1}\ldots\sigma_N^{2j-1}|e^{-\beta H_1/K}|\sigma_1^{2j}\ldots\sigma_N^{2j}\rangle\\&\quad\times\langle\sigma_1^{2j}\ldots\sigma_N^{2j}|e^{-\beta H_2/K}|\sigma_1^{2j+1}\ldots\sigma_N^{2j+1}\rangle,\end{aligned}\tag{2}$$

where the periodic boundary conditions along both spatial and temporal directions are assumed, i.e., $\sigma_i^1=\sigma_i^{2K+1}$ and $\sigma_1^j=\sigma_{N+1}^j$. Since the terms within $H_1$ (and $H_2$) mutually commute, Eq. (2) can be further decomposed as

$$Z_N\simeq\sum_{\{\sigma_i^j\}}\prod_{i=1}^{N/2}\prod_{j=1}^{K}v_{\sigma_{2i-1}^{2j-1}\sigma_{2i}^{2j-1},\sigma_{2i-1}^{2j}\sigma_{2i}^{2j}}v_{\sigma_{2i}^{2j}\sigma_{2i+1}^{2j},\sigma_{2i}^{2j+1}\sigma_{2i+1}^{2j+1}},\tag{3}$$

where the transfer matrix, $v_{\sigma_1\sigma_4,\sigma_2\sigma_3}\equiv\langle\sigma_1\sigma_4|\exp(-\beta h_{i,i+1}/K)|\sigma_2\sigma_3\rangle$, is a fourth-order tensor. Obviously, the partition function, Eq. (3), can be viewed as a classical transfer-matrix tensor network, as illustrated in Fig. 1(a).

 

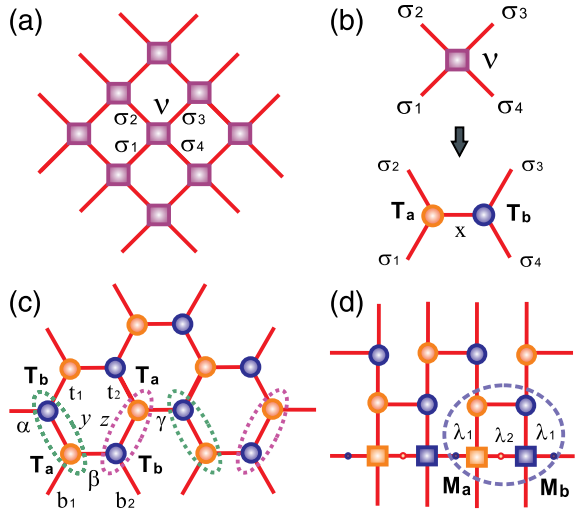


FIG. 1 (color online). (a) A transfer-matrix tensor network, where each bond denotes the $\sigma$ index in Eqs. (2) and (3). (b) A local transformation of a fourth-order tensor into two third-order tensors through a singular value decomposition (SVD). (c) Transform the transfer-matrix tensor network to a hexagonal one. (d) By contracting the intermediate bonds marked by dashed ovals in (c), one gets a brick wall structure with the fourth-order tensors in the bottom line.

The partition function can be obtained by summing over all the intermediate states $|\sigma_i^j\rangle$, namely, contracting all the bonds $\sigma$ in the tensor network. This procedure is accomplished by first making a singular value decomposition (SVD) of $\nu$ tensors in the following way:

$$\nu_{\sigma_1\sigma_2,\sigma_3\sigma_4} = \sum_{x=1}^{D^2} U_{\sigma_1\sigma_2,x}\lambda_x V^{\top}_{x,\sigma_3\sigma_4} \equiv \sum_{x=1}^{D^2} (T_a)_{x,\sigma_1,\sigma_2}(T_b)_{x,\sigma_3,\sigma_4}, \tag{4}$$

where the diagonal matrix $\lambda$ collects $D^2$ singular values, and two auxiliary tensors $(T_a)_{x,\sigma_1,\sigma_2} \equiv U_{\sigma_1\sigma_2,x}\sqrt{\lambda_x}$ and $(T_b)_{x,\sigma_3,\sigma_4} \equiv V_{\sigma_3\sigma_4,x}\sqrt{\lambda_x}$ are introduced for convenience. After this transformation, the square tensor network becomes a hexagonal one with two third-order tensors $T_a$ and $T_b$, as depicted in Fig. 1(b). Then, one contracts the $\sigma$ bonds encircled by the dashed oval lines between the last two rows in Fig. 1(c), which leads to the two fourth-order tensors

$$(M_a)_{\alpha,t_1,\beta,b_1} = \sum_{y=1}^{D}(T_a)_{\beta,b_1,y}(T_b)_{\alpha,t_1,y},$$
$$(M_b)_{\beta,t_2,\gamma,b_2} = \sum_{z=1}^{D}(T_a)_{\gamma,z,t_2}(T_b)_{\beta,z,b_2}, \tag{5}$$

which form a matrix product operator (MPO) lying in the bottom line of the whole tensor network, that can also be viewed as a "superket" in the operator Hilbert space [19]. Each horizontal bond between $M_a$ and $M_b$ is assigned with a diagonal matrix $\lambda_{1,2}$. Finally, we obtain a tensor network with brick wall structure as shown in Fig. 1(d).

Next, one can project the tensors $T_{a,b}$ onto $M_{a,b}$ successively. At each time, we project one row of tensors $T_a$ and $T_b$ followed by updating $M_{a,b}$ and $\lambda_{1,2}$. After two projections, the system evolves one Trotter step forward. This procedure is illustrated in Fig. 2. One first contracts the $\sigma$ bonds between $M$ tensors and $T$ tensors in Fig. 2(a) to obtain a sixth-order tensor in Fig. 2(b)

$$O_{y,\alpha,b_1,z,\gamma,b_2} = \sum_{x,t_1,t_2,\beta}(\lambda_1)_\alpha(M_a)_{\alpha,t_1,\beta,b_1}(\lambda_2)_\beta(M_b)_{\beta,t_2,\gamma,b_2} \times (\lambda_1)_\gamma(T_a)_{x,t_1,y}(T_b)_{x,z,t_2}, \tag{6}$$

and then takes a SVD of the $O$ tensors (after matricization). $O_{y\alpha b_1,z\gamma b_2} \simeq \sum_\beta^{D_c} U_{y\alpha b_1,\beta}(\lambda_2')_\beta V^{\top}_{\beta,z\gamma b_2}$, while keeping only the largest $D_c$ singular values of $\lambda_2'$. One can define new $M$ tensors $(M_a')_{\alpha,y,\beta,b_1} = U_{y\alpha b_1,\beta}/(\lambda_1)_\alpha$ and $(M_b')_{\beta,z,\gamma,b_2} = V_{z\gamma b_2,\beta}/(\lambda_1)_\gamma$, and update the horizontal bonds with $\lambda_2'$. After these operations, the last row of the tensor network is half updated as shown in Fig. 2(c). To project the next row of tensors, one can simply exchange $M_a$ and $M_b$ as well as $\lambda_1$ and $\lambda_2$ in Eq. (6). These two successive projections make up a full Trotter step $\tau$, as illustrated from Fig. 3(a) to Fig. 3(c). In each Trotter step, the transfer-matrix tensor network is decimated linearly with only $O(D_c)$ singular values discarded, which improves greatly the efficiency compared with the original TRG approach where $O(D_c^n)$ ($n = 2$ for honeycomb network) ones are discarded in the coarse-graining procedure [20].

In order to avoid the divergence in the imaginary time evolution, one has to normalize all the singular values in $\lambda$ with its largest one $n_i$ in $i$th step. After projecting all the $T$ tensors at inverse temperature $\beta$, one is left with the matrix product density operator of the present system. It consists of fourth-order $M$ tensors [see Fig. 3(c)], each of which has two legs with physical indices $t$ and $b$ in the Trotter direction, that can be further traced out due to the periodic boundary condition. Thus, we obtain a 1D matrix product extended in the spatial direction, where the matrices are labeled as $cM_{a,b}$ as shown in Fig. 3(d). It is convenient to assume the number of matrices is $2^p$. To get the trace of the

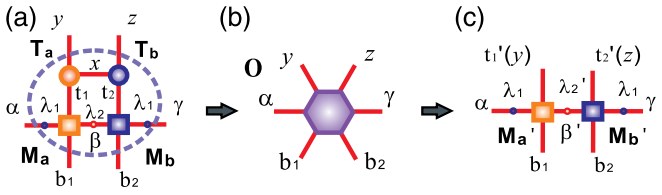


FIG. 2 (color online). A local evolution of the tensors by contraction and SVD. (a) Contract the intermediate bonds; (b) obtain a sixth-order tensor $O$; and (c) calculate the singular value decomposition (SVD) of $O$, and update the tensors $M_{a,b}$ and $\lambda$. The above manipulation has a computational cost that scales as $O(D^6D_c^3)$.

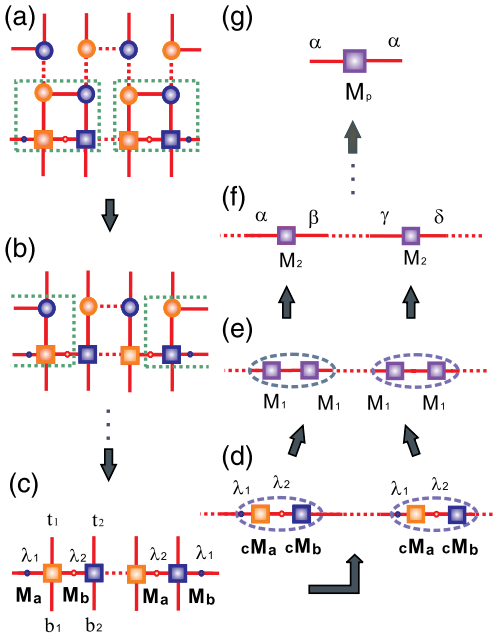


FIG. 3 (color online). An successive projection of each row of tensors onto the MPO in the bottom line [(a)–(c)]. After the projection along the Trotter direction, by tracing out the physical indices $t$ and $b$ of the MPO, one may get a 1D matrix product, of which the trace can be obtained by a matrix RG procedure [(d)–(g)].

product of these $2^p$ matrices, one can contract the neighboring matrices pairwise to obtain a new product of $2^{p-1}$ matrices, each of which should be normalized by the absolute value of its largest elements to avoid divergence. This contraction procedure is represented in Figs. 3(d)–3(g). After $p$ steps, the $2^p$ matrices shrink to a single one, of which the trace can be easily calculated. In each coarse-graining step, all the normalization factors denoted by $m_j$ with $j = 1, \cdots, p$ need to be collected for the calculation of physical quantities, e.g., the free energy per site $f$ at inverse temperature $\beta = K\tau$ can then be determined by the normalization factors $n_j$'s and $m_j$'s

$$f = -\frac{1}{\beta L}\ln\Big[\prod_{i=1}^{2K-2}(n_i)^{L/2}\prod_{j=1}^{p}(m_j)^{L/2^j}\Big]$$
$$= -\frac{1}{K\tau}\Big(\sum_{i=1}^{2K-2}\frac{\ln n_i}{2}+\sum_{j=1}^{p}\frac{\ln m_j}{2^j}\Big). \quad (7)$$

In the above descriptions, we illustrate the LTRG algorithm by first decimating the tensors along the Trotter direction, and then contracting the matrices in the spatial direction. Alternatively, one can also perform the decimation first in the spatial direction, and then do the matrix contraction in the Trotter direction.

As an example, we are going to demonstrate the efficiency of the LTRG algorithm by computing the free energy and other thermodynamic quantities of the quantum $XY$ spin-1/2 chain with a local Hamiltonian $h_{i,i+1} = -J(S_i^x S_{i+1}^x + S_i^y S_{i+1}^y)$ in Eq. (1) with $J = 1$. We take the

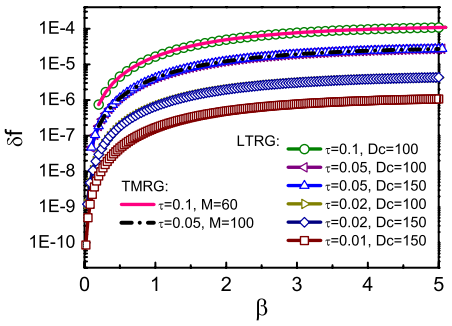


FIG. 4 (color online). The relative error of the free energy per site, $\delta f$, of the quantum $XY$ spin chain at high temperatures. $\delta f$ converges rapidly with $D_c$, and the lines with $D_c = 100$ and 150 coincide with each other ($\tau = 0.05, 0.02$). In addition, the TMRG results ($\tau = 0.1, 0.05$) are also presented for a comparison.

chain length to be $2^{100}$, which definitely reaches the thermodynamic limit.

In Fig. 4, we show the relative error of the free energy $f$ with respect to the exact solution, i.e., $\delta f = |(f - f_{\text{exact}})/f_{\text{exact}}|$, for different Trotter steps $\tau = 0.1, 0.05, 0.02, 0.01$. We observe that the accuracy is enhanced with decreasing $\tau$, as well as increasing $D_c$. Owing to the close relation between iTEBD and DMRG, the truncation parameter $D_c$ plays a role similar to the number of states kept $M$ in the TMRG method. As shown in Fig. 4, we compare the LTRG results to those of TMRG, both of which show the same accuracy for $\tau = 0.1$ and 0.05. It is also noticed that the relative errors saturate rapidly with increasing $D_c$, implying that the errors at high temperatures (e.g., $T > 0.2J$) mainly originate from the Trotter-Suzuki decomposition. In order to check the truncation error, the LTRG algorithm is also tested at very low temperatures. In Fig. 5, the temperature is down to $T = J/120$ with a Trotter step $\tau = 0.05$. As shown in Fig. 5(a), the accuracy of low $T$ results is remarkably improved by increasing $D_c$, and the relative error $\delta f \simeq 7 \times 10^{-6}$ at $\beta = 120$ for $D_c = 150$.

Besides the free energy, other thermodynamic quantities, such as the internal energy, can also be obtained. There are at least two ways to get them, one can either introduce some impurity tensors in the tensor network

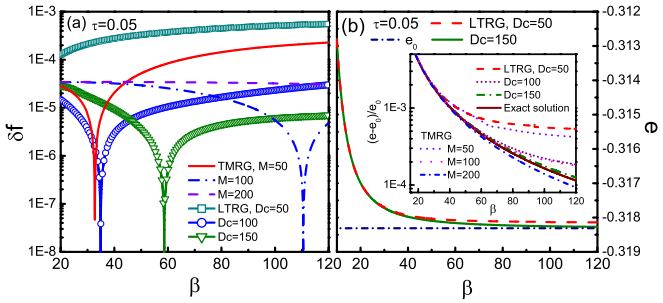


FIG. 5 (color online). LTRG and TMRG results of the quantum $XY$ spin chain. (a) Relative error of the free energy per site $\delta f$. (b) The energy per site $e$. The inset shows the variation of $(e - e_0)/e_0$ with inverse temperature $\beta$ for various $D_c$.

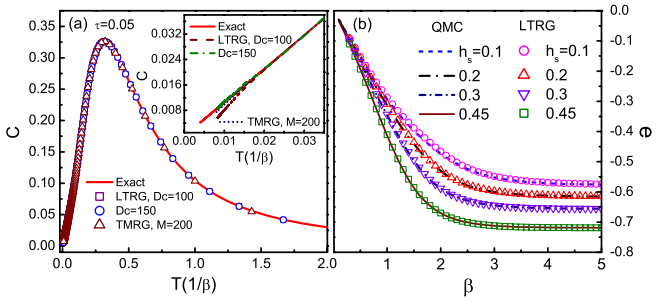


FIG. 6 (color online). (a) Specific heat as a function of temperature ($T = 1/\beta$) of the quantum $XY$ spin chain. The inset shows the low temperature results for $D_c = 100$ and 200, along with the TMRG data ($M = 200$) for a comparison. (b) Energy per site of the 2D spin-1/2 Heisenberg antiferromagnet on a honeycomb lattice for different staggered magnetic fields. The QMC results are obtained by using the ALPS library [21].

(see, for instance, Ref. [8]), or do a numerical differentiation of free energy with respect to temperature. Both ways are found to have a similar accuracy. In Fig. 5(b), the energy per site, $e$, is presented. We apply the LTRG algorithm to approach the ground state energy $e_0$, and find the difference $(e - e_0)/e_0$ is about $10^{-4}$ at $\beta = 120$ for $D_c = 150$, suggesting that the LTRG result is very close to the exact solution. The TMRG results with various $M$ (up to $M = 200$) are also included in Fig. 5 for a comparison. The relative errors for the free energy and internal energy are found to be of the same order down to $\beta = 120$ for both approaches.

The specific heat of the quantum $XY$ spin chain is also calculated, as shown in Fig. 6(a). The LTRG results agree quite well with the exact solution both at high and low temperatures. As indicated in the inset, the accuracy will be enhanced by increasing $D_c$. For $D_c = 150$, the LTRG results coincide with the exact solution down to very low temperature ($T/J \simeq 0.008$). The TMRG results with states $M = 200$ are also included, showing that both numerical methods have the comparable accuracy.

To examine the scalability of the LTRG algorithm, we also calculate the energy per site of a 2D spin-1/2 Heisenberg antiferromagnetic model on a honeycomb lattice, whose Hamiltonian is $H = J\sum_{\langle i,j\rangle}\vec{S}_i \cdot \vec{S}_j + h_s\sum_i (-1)^{|i|} S_i^z$, where $(-1)^{|i|}$ denotes the parity of the lattice and $h_s$ is a staggered magnetic field, as shown in Fig. 6(b). A pronounced agreement between LTRG and quantum Monte Carlo (QMC) results is clearly seen.

In summary, we have proposed a linearized TRG algorithm to calculate the thermodynamic properties of low-dimensional quantum lattice models, and obtained very accurate results. The LTRG algorithm can be readily generalized to fermion and boson models, and also provides a quite promising way to simulate the 2D quantum lattice models without involving the negative sign problem.

We are indebted to Q. N. Chen, J. W. Cai, J. Sirker, T. Xiang, Z. Y. Xie, and H. H. Zhao for stimulating discussions, and Z. Y. Chen, S. J. Hu, Y. T. Hu, G. H. Liu, X. L. Sheng, Y. H. Su, Q. B. Yan, and Q. R. Zheng for helpful assistance. This work is supported in part by the NSFC (Grants No. 10625419, No. 10934008, No. 10904081, and No. 90922033) and the Chinese Academy of Sciences.

*Corresponding author: gsu@gucas.ac.cn

[1] S. R. White, Phys. Rev. Lett. **69**, 2863 (1992); Phys. Rev. B **48**, 10345 (1993).
[2] U. Schollwoeck, Rev. Mod. Phys. **77**, 259 (2005); Ann. Phys. (Leipzig) **326**, 96 (2011).
[3] M. Levin and C. P. Nave, Phys. Rev. Lett. **99**, 120601 (2007).
[4] H. C. Jiang, Z. Y. Weng, and T. Xiang, Phys. Rev. Lett. **101**, 090603 (2008); Z. Y. Xie *et al.*, Phys. Rev. Lett. **103**, 160601 (2009); H. H. Zhao *et al.*, Phys. Rev. B **81**, 174411 (2010).
[5] Z. C. Gu, M. Levin, and X. G. Wen, Phys. Rev. B **78**, 205116 (2008); Z. C. Gu and X. G. Wen, Phys. Rev. B **80**, 155131 (2009).
[6] F. Verstraete and J. I. Cirac, arXiv:cond-mat/0407066.
[7] G. Vidal, Phys. Rev. Lett. **99**, 220405 (2007); Phys. Rev. Lett. **101**, 110501 (2008).
[8] G. Vidal, Phys. Rev. Lett. **98**, 070201 (2007); R. Orús and G. Vidal, Phys. Rev. B **78**, 155117 (2008).
[9] F. Verstraete, J. J. Garcia-Ripoll, and J. I. Cirac, Phys. Rev. Lett. **93**, 207204 (2004).
[10] A. E. Feiguin and S. R. White, Phys. Rev. B **72**, 220401 (2005); S. R. White, Phys. Rev. Lett. **102**, 190601 (2009); E. M. Stoudenmire and S. R. White, New J. Phys. **12**, 055026 (2010).
[11] M. Suzuki and M. Inoue, Prog. Theor. Phys. **78**, 787 (1987); M. Inoue and M. Suzuki, Prog. Theor. Phys. **79**, 645 (1988).
[12] M.-C. Chang and M.-F. Yang, Phys. Rev. B **79**, 104411 (2009).
[13] W. Li *et al.*, Phys. Rev. B **82**, 134434 (2010).
[14] P. Chen, C. Y. Lai, and M. F. Yang, J. Stat. Mech. (2009) P10001.
[15] W. Li *et al.*, Phys. Rev. B **81**, 184427 (2010).
[16] R. J. Bursill, T. Xiang, and G. A. Gehring, J. Phys. Condens. Matter **8**, L583 (1996); Xiaoqun Wang and Tao Xiang, Phys. Rev. B **56**, 5061 (1997); Tao Xiang, Phys. Rev. B **58**, 9142 (1998).
[17] B. Gu, G. Su, and S. Gao, Phys. Rev. B **73**, 134427 (2006); B. Gu and G. Su, Phys. Rev. Lett. **97**, 089701 (2006); B. Gu and G. Su, Phys. Rev. B **75**, 174437 (2007); S.-S. Gong, S. Gao, and G. Su, Phys. Rev. B **80**, 014413 (2009); S.-S. Gong *et al.*, Phys. Rev. B **81**, 214431 (2010).
[18] J. Sirker, Phys. Rev. B **73**, 224424 (2006); J. Sirker, J. Damerau, and A. Klumper, Phys. Rev. B **78**, 235125 (2008); J. Sirker, Phys. Rev. B **81**, 014419 (2010); J. Sirker, Phys. Rev. Lett. **105**, 117203 (2010).
[19] M. Zwolak and G. Vidal, Phys. Rev. Lett. **93**, 207205 (2004).
[20] We note that the present LTRG algorithm can also be applied to evaluate the thermodynamics of 2D classical models, achieving more accurate results than the coarse-graining TRG algorithm.
[21] A. F. Albuquerque *et al.*, J. Magn. Magn. Mater. **310**, 1187 (2007).